Post-print of: Szymon Winczewski, Mohamad Yousef Shaheen, Jarosław Rybicki, Interatomic potential suitable for the modeling of penta-graphene: Molecular statics/molecular dynamics studies, Carbon, Volume 126, 2018, Pages 165-175, https://doi.org/10.1016/j.carbon.2017.10.002.

Interatomic Potential Suitable for the Modeling of Penta-graphene: Molecular Statics/Molecular Dynamics Studies

Szymon Winczewski[a,*], Mohamad Yousef Shaheen[b], Jarosław Rybicki[a,c]

[a] *Faculty of Applied Physics and Mathematics, Gdansk University of Technology, Narutowicza 11/12, 80-233 Gdańsk, Poland.*
[b] *Faculty of Engineering Technology, University of Twente, Drienerlolaan 5, 7522 NB Enschede, The Netherlands*
[c] *TASK Computer Centre, Gdansk University of Technology, Narutowicza 11/12, 80-233 Gdańsk, Poland*

Abstract

We test the potentials available for elemental carbon, with the scope to choose the potential suitable for the modeling of penta-graphene, the latest two dimensional carbon allotrope. By using molecular statics and molecular dynamics simulations we show that there is only one potential – namely the Tersoff-type potential proposed by Erhart and Albe in 2005 – which is able to correctly describe all the important features of penta-graphene. We show that this potential gives structural, mechanical and energetic parameters which are in accordance with the previously reported *ab initio* results.

1. Introduction

The synthesis of carbon nanotubes in 1992 [1, 2] and the discovery of graphene in 2004 [3, 4] have opened a completely new area of search for new carbon allotropes. Based on theoretical considerations many new carbon forms have been proposed since then, and as a result, the set of known carbon forms has been enriched by several low-dimensional [5–11] and bulk [12–16] structures. Despite the fact that many of these structures have not been synthesized yet, this new trend has shown the importance of theoretical studies – especially *ab initio* quantum mechanical calculations – for the search for new materials of designed properties, often unique.

*Corresponding author
Email address: wisnia@kdm.task.gda.pl (Szymon Winczewski)

The fact that most of the carbon allotropes have a structure consisting of hexagons as its main feature, has motivated the search for a new carbon allotrope which would have a structure completely composed of pentagons. As a result a new two-dimensional carbon allotrope, called penta-graphene, was proposed by Zhang *et al.* in 2014 [9], as an „exfoliated equivalent" of the T12-carbon [12], the existence of which was also predicted based on the *ab initio* calculations.

Penta-graphene (PG) can be seen as a layer of pentagons constructed from a mixture of sp^2- and sp^3-bonded carbon atoms. Zhang *et al.* reported that due to its unusual atomic structure – closely resembling the well-known Cairo pentagonal tiling – PG possesses many unique properties. It was found to be mechanically, dynamically and thermally stable, and able to withstand temperatures as high as $T = 1000$ K. It was also reported that PG displays ultra-high mechanical strength, with the strain at maximum stress being as high as 21%. The stiffness of PG was also found to be very high, with the corresponding (in-plane) Young's modulus being as high as $E = 263$ GPa nm, which is more than two-thirds of that of graphene ($E = 345$ GPa nm). PG was also found to exhibit auxetic behavior, that is the anomalous property of becoming wider rather than thinner when stretched. Zhang *et al.* also reported that PG exhibits an intrinsic (and indirect) band gap, as large as $E_g = 3.25$ eV. This feature renders PG as a better material – than graphene – for two-dimensional transistors, which require the presence of a large band gap to obtain a good switch-off.

1.1. State of the art

Since its discovery PG has been studied intensively by several groups [11, 17–29]. The stability of PG and its experimental reachability was questioned by Ewels *et al.* in [17]. Based on the *ab initio* calculations they concluded that PG should be difficult to isolate, also pointing out that PG should rapidly restructure toward graphene in the presence of even a few catalytic impurities. A similar observation about the potential instability of PG was made by Cranford [18], who studied finite, hydrogen-terminated sheets of PG. By using the MD simulation he concluded that bond breaking should be observed even at relatively small deformations (*ca.* 5%),

leading to transformations of pentagons into hexagons and heptagons. According to his work, a similar effect should be observed at elevated temperatures (*ca.* 600 K), resulting in transformation of PG into (defective) graphene.

Sun *et al.* [11] presented the results of extensive studies on the mechanical properties of PG. By combining DFT calculations with the fourth order continuum elasticity theory they calculated a complete set of (fifteen) anisotropic nonlinear elastic constants of monolayer PG, showing that the applied continuum formalism (originally proposed by Wei *et al.* for graphene [30]) is able to accurately describe the non-linear elastic behavior of PG in a wide range of strains, even as large as 30%. Sun *et al.* also investigated the fracture of PG. They concluded that due to longer bond length and lower charge density the sp^3 bonds are more vulnerable to failure than the sp^2 bonds. Sun *et al.* also studied the mechanism of PG deformation, demonstrating that the negative Poisson's ratio of PG originate from de-wrinkling of different atomic planes.

The influence of doping and functionalization on the properties of PG has been also investigated. Berdiyorov *et al.* [19] found that electronic properties of PG can be fine-tuned, by substituting C atoms with Si, B and N. They showed that the band gap size can be significantly reduced, even to 0.2 eV. According to them the strongest reduction of the band gap is obtained for Si substitutions on the top (or bottom) plane of PG. They also showed that surface termination with fluorine and hydroxyl groups results in an increase in the band gap. The functionalization of PG sheets was also investigated by Li *et al.* [20], who found that hydrogenation and fluorination can effectively tune the electronic and mechanical properties of PG, changing the Poisson's ratio from negative to positive, and reducing the Young's modulus.

The thermal conductivity of PG has been also studied. Using classical equilibrium molecular dynamics (MD), Xu *et al.* [21] found that the thermal conductivity of PG at the room temperature is about 170 W/(m K), which is much lower than that of graphene, which is 2000-4000 W/(m K) [31]. They also identified the main mechanism of thermal conduction. By analyzing phonon frequencies and phonon mean free paths they found out that the acoustic phonons make a contribution

of about 90% to the thermal conductivity, also showing that phonons with mean free paths larger than 100 nm make a contribution over 50%. They have also demonstrated that the remarkably lower thermal conductivity of PG (compared with graphene) results from the lower phonon group velocities and fewer collective phonon excitations.

The influence of functionalization on the thermal properties of PG has been also studied. Using DFT calculations combined with an iterative solution of the phonon Boltzmann transport equation, Wu *et al.* [22] found that hydrogenation of PG leads to large (76% increase) improvement in thermal conductivity.

Other spatial forms of PG have been also investigated. Yu and Zhang studied the electronic properties of layered PG [23]. They showed that there is no direct-to-indirect band gap transition in PG by varying strain, layer number, and stacking misalignment. Owing to its characteristics, few-layer PG was recognized by Yu and Zhang [23] as a very promising material for optoelectronic and photovoltaic applications. Recently, Rajbanshi *et al.* [24] by using DFT studied penta-graphene nanoribbons (PGNRs), concluding that PGNRs are thermodynamically meta-stable with respect to graphene nanoribbons. They also found that on application of uniaxial strain the band gap of PGNRs decreases continuously, yielding a strain-tunable optoelectronic material.

Another potential application of PG has been recently highlighted by Xiao *et al.* [25]. By using DFT calculations they found that PG provides very high ion storage capacity and fast ion diffusivity, and therefore is a promising anode material for the Li/Na-ion batteries.

1.2. Problem statement

The above presented analysis of the current state of knowledge shows how significant the future role of PG may be. At the same time, it illustrates the increasing importance of atomistic modeling techniques. So far, the DFT methods have been mainly used in studies on PG and – to the best of our knowledge – there are only three papers, which have reported the application of empirical potentials to model PG [18, 21, 26].

In the first article Cranford [18] has employed the reactive force field [32] (REAX) to study the mechanical properties and the chemical stability of PG, while in the second Ebrahimi [26] has used the reactive empirical bond order (REBO) potential [33] to study the effect of hydrogen coverage on the buckling of PG. It is important to note that no preliminary validation of the chosen description method has been carried out in both of the aforementioned works.

Contrary to this, Xu *et al.* [21] performed such validation by testing four different interatomic potentials: the original Tersoff potential [34, 35], the optimized Tersoff potential [36, 37], the REBO potential [33] and the environment-dependent interatomic potential [38] (EDIP). By comparing the calculated structural and mechanical parameters with the results of the *ab initio* calculations they concluded that among the tested interaction models the original Tersoff potential most closely reproduces the properties of PG. Therefore, it was used in [21] to study the transport phenomena in PG. However, it must be noted that the Poisson's ratio of PG calculated with the use of the original Tersoff potential was found in [21] to be equal to -0.174, which strongly (more than 2.5-times) differs from the *ab initio* result of Zhang *et al.* [9], which is -0.068. Such a significant difference suggests that the original Tersoff potential may not be the best choice when modeling PG at the empirical level.

It is well known that the credibility of the results obtained from any atomistic simulation depends first and foremost on the quality of the model employed to describe interatomic interactions. The last three decades have brought significant advances in the development of empirical potentials. This is especially true in the case of carbon. Due to the significance of this element for the nanotechnology revolution, many new potentials have been proposed for carbon [32–52], in order to describe its various – and often very different – forms. Since all potentials for carbon have been parameterized without accounting for the properties of PG – which was unknown when the potentials were developed – before starting modeling PG at the empirical level it is important to first test how well, or whether at all, the existing potentials reproduce the properties of this new – and very exotic – form of carbon.

It must be stressed that the unusual structure of PG makes this system some-

how challenging for the empirical potentials. This originates from the fact that there are two types of bonding schemes present in PG, with the entire structure being a „mixture" of sp^2- and sp^3-hybridized atoms. This is a reason why the basic building blocks in PG differ significantly from their counterparts seen in diamond and graphite/graphene (*e.g.* the carbon-carbon bond lengths characteristic for diamond and graphite/graphene are 1.54 Å and 1.42 Å, respectively, the corresponding bonds in PG have the lengths of 1.55 Å and 1.34 Å, respectively, also the valence angles typical for PG – *i.e.* 98.6, 112.2, 113.5 and 134.4 degrees – differ significantly from those typical for diamond – 109.5 degrees — and graphite/graphene – 120 degrees). Therefore, it is not clear if even the potentials, which are known as being able to (simultaneously) describe purely sp^2- and purely sp^3-systems, will be able to correctly capture the characteristics of PG.

The above observations led us to start the studies the results of which are presented in this paper. We considered 14 different empirical potentials available for carbon and based on molecular statics/molecular dynamics (MS/MD) simulations tested if any of them is able to describe (at least in a satisfactory manner) the interactions in this unusual system, possessing exotic, sp^2-sp^3 mixed hybridization, not seen in typical carbon forms.

This paper is organized as follows. In Section 2 we describe the structure of PG and recap the results of the *ab initio* calculations of Zhang *et al.* [9]. We also briefly present the interatomic potentials that were tested in this work. In Section 3 we present the results of MS calculations of structural, energetic and mechanical properties of PG and compare the results obtained with different empirical potentials against the results of Ref. [9]. On this basis, we choose the most promising interatomic potential for further validation. Section 4 is devoted to a presentation of studies on the finite temperature stability of PG performed on the basis of MD simulation. We conclude with a summary in Section 5.

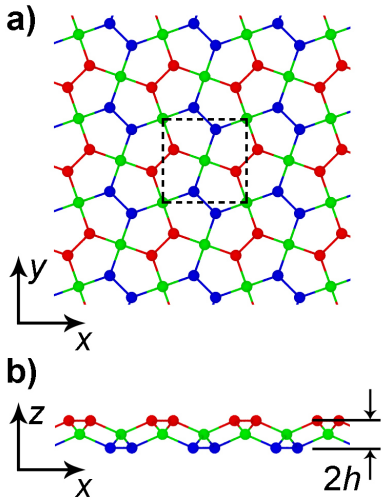

Figure 1: Structure of penta-graphene: top (panel a) and side (panel b) views. C1 atoms are represented by green spheres, while C2 atoms are depicted in blue (lower layer) and red (upper layer). The unit cell of penta-graphene is marked with the dashed square. The illustration was generated using OVITO [53].

2. Theoretical

2.1. Structure of penta-graphene

The structure of PG (as described by Zhang *et al.* in [9]) is presented in Figure 1. PG possesses $P\text{-}42_1m$ symmetry (space group number 113) with a tetragonal lattice. Its unit cell has the lattice parameters $a = b = 3.64$ Å and contains two types of carbon atoms: sp^3- (later on termed as C1 atoms) and sp^2-bonded (C2 atoms). Effectively, the unit cell of PG contains two C1 atoms and four C2 atoms.

PG has a layered structure, with three layers present (see Figure 1b). The C1 atoms are lying on the middle layer with $z = 0$, and the C2 atoms are forming two external layers with $z = \pm h$. Here, h denotes the interlayer spacing which – according to Ref. [9] – equals to 0.6 Å. The C1 atoms serve as connectors: each of them is connected to four C2 atoms, two from each outer layer. Each of the C2 atoms is connected to two C1 atoms and one C2 atom from the same outer layer.

There are two types of bonds in PG: C1-C2 bonds – which all have the same length $d_1 = 1.55$ Å – and C2-C2 bonds – all with the length $d_2 = 1.34$ Å. All pentagons are the same and their interior angles are equal to 113.5 (C1-C2-C2

angle, occurs twice), 112.4 (C1-C2-C1 angle) and $\theta_1 = 98.6$ degrees (C2-C1-C2 angle, also occurs twice). There is also another C2-C1-C2 angle, which measures PG crumpling. According to Ref. [9] it is equal to $\theta_2 = 134.4$ degrees.

The geometry of PG slightly differs from that of the Cairo pentagonal tiling, which is strictly two-dimensional. For the latter the interior angles are equal to 120 (occurs three times) and 90 degrees (occurs twice), and the ratio of the pentagon shorter edge to its longer edge is $\sqrt{3} - 1 \approx 0.73$, while for PG it is $d_2/d_1 \approx 0.86$.

Since PG has tetragonal symmetry its in-plane mechanical properties can be described with three independent elastic constants: C_{11}, C_{12} and C_{66}. Here, we have employed the Voigt notation which will be used throughout this paper. Knowing the elastic constants one may easily calculate the Young's modulus E and the Poisson's ratio ν, using the following formulas:

$$E = \frac{C_{11}^2 - C_{12}^2}{C_{11}} \tag{1}$$

and

$$\nu = \frac{C_{12}}{C_{11}}. \tag{2}$$

In the case of the tetragonal lattice both of the above moduli depend on the direction of measurement. The presented formulas correspond to the $< 1, 0 >$ family of directions. The elastic constant C_{66} defines the shear modulus $\mu = C_{66}$. Ref. [9] reported that $C_{11} = 265$ GPa nm, $C_{12} = -18$ GPa nm and $C_{66} = 152$ GPa nm.

2.2. Considered interatomic potentials

In this work, we considered 14 different interatomic potentials available for carbon. We limited ourselves to those potentials for which there were indications that they may be able to reliably describe PG. The full list of the tested potentials is given in Table 1, where the potentials are grouped into four classes, according to their characteristics.

The first class groups potentials of the Tersoff type [54]. In addition to the original Tersoff potential [34, 35] (denoted as T89), there are two other parameterizations: a parameterization by Erhart and Albe [39] (T05), designed for simulations of bulk carbon (diamond and graphite) and silicon carbide, and a parameterization

by Lindsay and Broido [36, 37] (T10), which was developed to simulate carbon nanotubes and graphene.

The second class comprises two potentials of the Stillinger-Weber type [55, 56]: the original parameterization for carbon (denoted as SW) proposed by Mahon *et al.* [40], and the improved version (denoted as ISW) proposed by Barnard and Russo [41]. Both of them were parameterized for tetrahedral carbon.

The third class comprises the so-called reactive potentials and there are six potentials in this class, which can be further divided into two subclasses.

The first subclass comprises the REBO potential [33] and its improved version, *i.e.* the adaptive intermolecular reactive empirical bond order potential [44] (AIREBO). Both of them were shown to be successful in describing various carbon allotropes, including diamond, graphite and graphene. We note that the REBO potential considered in this work corresponds to the so-called 2nd generation REBO proposed by Brenner *et al.* in 2002, not the original REBO from 1990 [42]. We also tested the recently developed AIREBO-M potential [45] which is a modification of the AIREBO potential, wherein the singular Lennard-Jones term was replaced with a Morse-type potential, in order to improve the description of highly compressed molecular configurations. The fact that the C2-C2 bonds in PG are much shorter than typically in our opinion justifies the use of this potential.

The second subclass contains various parameterizations of the reactive force field originally proposed by van Duin *et al.* [46]. In general, in the literature there are more than 10 parameterizations of this force-field available that allow describing C-C interactions [32, 46–48, 57–62] (a good overview of the REAX methodology, its various branches and their applicability is provided in [63]). However, most of them have been designed to model multicomponent organic compounds and have not been tuned to describe interactions in pure carbon systems. In this study, we limited ourselves to those, for which the properties of pure carbon were taken into account during the parameterization procedure, and which – consequently – might be successful in describing PG. Therefore, we tested the following parameterizations: a parameterization by Nielson *et al.* [47] (which was developed to study the catalytic formation of carbon nanotubes), a parameterization by Chenoweth *et al.* [32] (which

was already used by Cranford [18] to study mechanical properties and stability of PG and was found to be particularly successful), and a recent parameterization by Srinivasan *et al.* [48] (which was created to model condensed phases of carbon).

The last class comprises three potentials that do not fit into any of the previous groups. These are: the modified embedded atom method (MEAM) potential [49], the long-range carbon bond order potential (LCBOP) [50], and the analytical bond order potential (ABOP) [51]. The LCBOP potential was originally used to study diamond to graphite transformation [50]. For the ABOP potential – which was designed to model graphene, graphite and carbon nanotubes – it was also demonstrated that it is able to correctly describe the transformation of graphite to diamond at high pressures [51]. The choice of the MEAM potential can be justified by the fact that its parameterization accounted for the properties of diamond and graphite structure.

It is worth noting, that despite the fact that the studied potentials differ significantly in many aspects (this is especially true if one compares potentials from different groups defined), at the same time they are very similar in many aspects. Many of them are based on the concept of the bond order which was introduced in 1939 by Coulson [64], and for the first time applied in the context of computer atomistic simulation by Tersoff in 1986 [65]. This approach is crucial for describing systems with many different types of bonding, as it allows the covalent bonding interactions to adapt to the local chemical environment.

In this work, we do not seek to identify the particular features that would make individual potentials more appropriate for studying PG. Due to the large complexity of the functional forms that define the studied potentials, we also do not present a more detailed description of the underlying formalisms, referring the interested reader to the original works where the potentials were presented. However, some important observations that we have made during our selection of the potential suitable for PG will be presented later in this article.

Type/symbol	Year	Author(s) and reference
Tersoff type potentials		
T89	1989	Tersoff [34, 35]
T05	2005	Erhart and Albe [39]
T10	2010	Lindsay and Broido [36, 37]
Stillinger-Weber type potentials		
SW	1991	Mahon, Pailthorpe and Bacskay [40]
ISW	2013	Barnard and Russo [41]
Reactive potentials		
AIREBO	2000	Stuart, Tutein and Harrison [44]
REBO	2002	Brenner *et al.* [33]
AIREBO-M	2015	O'Connor, Andzelm and Robbins [45]
REAX05	2005	Nielson *et al.* [47]
REAX08	2008	Chenoweth *et al.* [32]
REAX15	2015	Srinivasan, van Duin and Ganesh [48]
Other potentials		
MEAM	1992	Baskes [49]
LCBOP	2003	Los and Fasolino [50]
ABOP	2015	Zhou, Ward and Foster [51]

Table 1: Tested interatomic potentials.

3. Molecular Statics calculations

3.1. Validation procedure

In order to test the reliability of the considered potentials for each of them have calculated the structural and mechanical properties of PG at $T = 0$ K, using the MS technique. In choosing the most reliable potential we followed a practical approach, whereby we compared the obtained results with the *ab initio* calculations of Zhang *et al.* [9], which were taken as a reference. Our test set consisted of the following structural properties: the lattice parameter a; the interlayer spacing h; two lengths of C-C bonds, d_1 and d_2 respectively; two valence angles, θ_1 and θ_2 respectively. We also examined the mechanical properties, by calculating three elastic constants, C_{11}, C_{12} and C_{66}, and two elastic moduli, the Young's modulus E and the Poisson's

ratio ν. We also examined the relative stability of PG by calculating its binding energy E_{b}.

At the beginning we performed structure optimization in order to determine the equilibrium structure of PG at $T = 0$ K. The minimization was started taking the *ab initio* result of [9] as an initial configuration and involved repeated, alternating optimization of the box and atomic coordinates in order to obtain a structure that corresponds to the minimum of energy, zero (negligible) stress tensor and zero (negligible) forces acting on individual atoms. Strict convergence criteria were used. The termination criterion was for all atomic force components to be below 10^{-8} eV Å^{-1}, with final positions being accurate to no worse than 10^{-6} Å. Minimization was carried out using the Polak-Ribiére [66] formulation of the conjugate gradient method.

In addition, the entire minimization procedure was repeated for different initial structures, that differed in the initial values of the lattice parameter a and the interlayer spacing h. This was done in order to check if there are any other local minima of potentially lower energy which are not accessible by means of local minimization when starting the optimization with the *ab initio* result. We tested 31×17 equispaced points in the (a, h) search space, with 3.34 Å $\leq a \leq$ 3.94 Å and 0.43 Å $\leq h \leq$ 2.16 Å.

All the calculations described here (and hereafter) were performed using the LAMMPS (large-scale atomic/molecular massively parallel simulator) simulation package developed by Plimpton *et al.* at Sandia [67]. The calculations were performed for the system consisting of 10×10 repetitions of the six-atom elementary cell, with the total number of atoms $N_{\mathrm{pg}} = 600$. Periodic boundary conditions (PBC) were applied along x and y directions. The non-periodic boundary condition was used along the z direction.

A similar methodology was applied for graphene, to determine its equilibrium state. This allowed us to examine the stability of PG with respect to graphene. The binding energy E_{b} of PG was calculated as

$$E_{\mathrm{b}} = \frac{E_{\mathrm{pg}}}{N_{\mathrm{pg}}} - \frac{E_{\mathrm{g}}}{N_{\mathrm{g}}}. \tag{3}$$

Here, E_{pg} (and E_{g}) denotes the potential energy of PG (and graphene) at the equilibrium state, while N_{pg} (and N_{g}) represents the total number of atoms in simulated PG (and graphene, which was taken as $N_{\mathrm{g}} = 448$).

After determining the equilibrium structure, elastic constants were calculated. For this purpose, we have calculated the dependence of the elastic energy $\Delta E = E - E_0$ on the strain. Here, E_0 and E denote the potential energies of equilibrium (unstrained) and strained system, respectively. Three different deformations were considered: the equibiaxial strain with $\varepsilon_1 = \varepsilon_2 = x$ (later denoted by D_1), the volume preserving biaxial strain with $\varepsilon_1 = [(1+x)/(1-x)]^{1/2} - 1$ and $\varepsilon_2 = [(1-x)/(1+x)]^{1/2} - 1$ (later denoted by D_2), and the shear strain with $\varepsilon_6 = x$ (later denoted by D_3).

The equilibrated (*i.e.* corresponding to the zero strain) structure was deformed by incrementally dilating the simulation box along the loading direction and applying an equal affine transformation to the atomic positions. This was followed by the energy minimization of the atomic coordinates. For each deformation type the elastic energy was calculated for 41 different values of x, equally spaced in the interval $[-0.005, 0.005]$. Such an approach allowed us to obtain well-behaving (*i.e.* clearly quadratic) strain–energy dependencies.

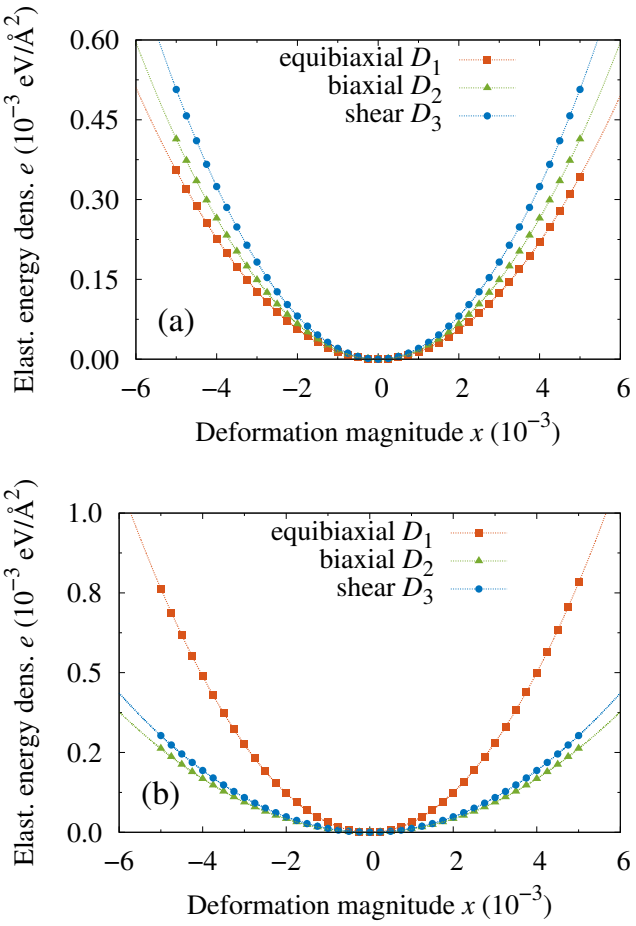

Figure 2: Elastic energy–strain relationships calculated for T05 (panel a) and REAX08 (panel b) potentials. Dashed lines represent obtained quadratic fits.

The first two deformations were used to calculate C_{11} and C_{12} elastic constants. For such deformations one obtains the following expressions for the elastic energy density e, written in terms of the elastic constants C_{11} and C_{12} and the magnitude of the applied strain x:

$$e = \Delta E/A_0 \approx (C_{11} + C_{12})\ x^2 \tag{4}$$

for deformation D_1, and

$$e = \Delta E/A_0 \approx (C_{11} - C_{12})\ x^2 \tag{5}$$

for deformation D_2. Here, A_0 denotes the surface area of the unstrained system. The last deformation (D_3) allowed us to calculate C_{66}, since the following equation is obtained for it:

$$e = \Delta E/A_0 \approx \frac{1}{2}\ C_{66}\ x^2. \tag{6}$$

Examples of $e(x)$ curves, obtained for the T05 and REAX08 potentials, are presented in Figure 2. Having all the elastic constants C_{11}, C_{12} and C_{66} we calculated the Young's modulus E and the Poisson's ratio ν, using equations (1) and (2).

3.2. Results

We start the presentation of the results with the obtained structural parameters, which are summarized in Table 2. Even a first glance shows that seven potentials have failed in describing the layering of PG, returning completely wrong (T10, AIREBO, REBO, AIREBO-M) or significantly overestimated (SW, ISW, MEAM) interlayer spacing h. This simple observation allows us to exclude the mentioned potentials from the further considerations. The remaining potentials were able to correctly capture the considered feature, giving the relative error smaller than 20% (or comparable to: ABOP), with the best agreement obtained for the three REAX potentials.

Potential	a (Å)	h (Å)	d_1 (Å)	d_2 (Å)	θ_1 (degrees)	θ_2 (degrees)	E_b (eV/atom)
ab initio	3.64	0.6	1.55	1.34	98.6	134.2	0.761
Tersoff type potentials							
T89	3.640 (-0.014)	0.683 (14)	1.555 (0.35)	1.483 (11)	101.1 (2.5)	127.9 (-4.7)	1.159 (52)
T05	3.592 (-1.3)	0.706 (18)	1.546 (-0.25)	1.483 (11)	102.0 (3.4)	125.7 (-6.4)	0.923 (21)
T10	3.944 (8.3)	0 (-100)	1.551 (0.083)	1.429 (6.6)	90.0 (-8.7)	180 (34)	1.371 (80)
Stillinger-Weber type potentials							
SW	3.467 (-4.7)	0.850 (42)	1.557 (0.46)	1.557 (16)	107.3 (8.8)	113.9 (-15)	-0.836 (-210)
ISW	3.459 (-5.0)	0.855 (42)	1.557 (0.44)	1.558 (16)	107.6 (9.0)	113.4 (-16)	-0.817 (-207)
Reactive potentials							
AIREBO	3.930 (8.0)	0.078 (-87)	1.576 (1.7)	1.301 (-2.9)	90.1 (-8.6)	174.3 (30)	1.043 (37)
REBO	3.936 (8.1)	0 (-100)	1.577 (1.7)	1.299 (-3.0)	90.0 (-8.7)	180 (34)	1.053 (38)
AIREBO-M	3.962 (8.9)	0.079 (-87)	1.585 (2.3)	1.327 (-0.97)	90.1 (-8.6)	174.3 (30)	0.859 (13)
REAX05	3.625 (-0.40)	0.624 (4.0)	1.542 (-0.52)	1.388 (3.6)	99.4 (0.83)	132.3 (-1.4)	0.986 (30)
REAX08	3.728 (2.4)	0.578 (-3.6)	1.558 (0.55)	1.440 (7.5)	97.9 (-0.70)	136.4 (1.7)	0.981 (29)
REAX15	3.487 (-4.2)	0.612 (2.0)	1.482 (-4.4)	1.368 (2.1)	99.8 (1.2)	131.2 (-2.2)	1.061 (39)
Other potentials							
MEAM	3.850 (5.8)	0.921 (53)	1.715 (11)	1.744 (30)	106.8 (8.3)	115.0 (-14)	-0.679 (-190)
LCBOP	3.635 (-0.13)	0.647 (7.9)	1.545 (-0.33)	1.446 (7.9)	100.1 (1.5)	130.5 (-2.8)	1.188 (56)
ABOP	3.437 (-5.6)	0.728 (21)	1.505 (-2.9)	1.414 (5.5)	103.5 (5.0)	122.2 (-9.0)	1.032 (36)

Table 2: Structural and energetic parameters of penta-graphene as predicted by various empirical potentials. For the convenience of comparison, the results of the *ab initio* calculations [9] are also presented. The reference value of the binding energy E_b has been taken from [17]. The value in the bracket represents the signed relative error (in percents). The strongly erroneous results have been highlighted in red. The criterion of the error being not greater than 5% (a), 25% (h), 0.05 Å (d_1), 0.1 Å (d_2), 5% (θ_1), 5% (θ_2) and 30% (E_b) has been used in coloring. The symbol of the potential has been highlighted in red if the potential returned (at least) one strongly erroneous result. The introduced coloring is an auxiliary construct meant as a guide for the eye, introduced to quickly highlight the potentials that we found to be decidedly unacceptable.

Potential	C_{11}	C_{12}	$C_{66} = \mu$	E	ν
ab initio	265	-18.0	152	264	-0.068
Tersoff type potentials					
T89	212 (-20)	-36.8 (104)	152 (-0.062)	205 (-22)	-0.174 (156)
T05	244 (-7.9)	-20.6 (15)	162 (6.7)	242 (-8.1)	-0.085 (24)
T10	320 (21)	33.7 (-287)	97.1 (-36)	316 (20)	0.105 (-255)
Stillinger-Weber type potentials					
SW	300 (13)	103 (-675)	202 (33)	264 (0.062)	0.345 (-608)
ISW	236 (-11)	29.1 (-262)	136 (-10)	232 (-12)	0.124 (-282)
Reactive potentials					
AIREBO	324 (22)	36.2 (-301)	7.83 (-95)	320 (21)	0.112 (-264)
REBO	321 (21)	36.8 (-305)	7.06 (-95)	317 (20)	0.115 (-269)
AIREBO-M	309 (17)	39.0 (-317)	6.96 (-95)	304 (15)	0.126 (-286)
REAX05	229 (-14)	93.2 (-618)	86.5 (-43)	191 (-27)	0.407 (-699)
REAX08	331 (25)	163 (-1007)	96.9 (-36)	250 (-5.1)	0.493 (-826)
REAX15	159 (-40)	41.8 (-332)	67.3 (-56)	148 (-44)	0.264 (-488)
Other potentials					
MEAM	115 (-57)	31.0 (-272)	79.6 (-48)	107 (-60)	0.270 (-497)
LCBOP	236 (-11)	-10.9 (-39)	216 (42)	235 (-11)	-0.046 (-32)
ABOP	312 (18)	-21.6 (20)	187 (23)	311 (18)	-0.069 (1.8)

Table 3: Mechanical properties of penta-graphene as predicted by various empirical potentials. The elastic constants C_{11}, C_{12}, C_{66} and the Young's modulus E are expressed in units of GPa nm. For the convenience of comparison, the results of the *ab initio* calculations [9] are also presented. The value in the bracket represents the signed relative error (in percents). The strongly erroneous results have been highlighted in red. For all quantities the same criterion of the relative error being not greater than 25% has been used in coloring. The symbol of the potential has been highlighted in red if the potential returned (at least) one strongly erroneous result. The introduced coloring is an auxiliary construct meant as a guide for the eye, introduced to quickly highlight the potentials that we found to be decidedly unacceptable.

Inspection of the calculated d_1 and d_2 bond lengths reveals another important failure, which is seen in the case of the Stillinger-Weber type potentials (SW and ISW) and the MEAM potential. These potentials returned identical d_1 and d_2 bond lengths, being unable to correctly recognize the differences seen in the neighborhoods of the sp^2- and sp^3-hybridized carbon atoms. Since this feature is very important for the modeling of the behavior of PG it is another argument for not choosing the SW, ISW and MEAM potentials.

For the not-yet-rejected seven potentials a good agreement with the *ab initio* calculations was reached. The LCBOP potential and the three REAX potentials significantly outperform the other potentials in describing the structural parameters of PG. Only for this four potentials none of the reported relative errors exceeded 10%. Therefore it is concluded that the LCBOP potential or the REAX potentials should be the potential of choice, when modeling PG and taking the structural parameters as the main indicator of the potential's quality. However, it should be noted that this statement does not exclude from further considerations the other three potentials, *i.e.* T89, T05 and ABOP, which were able to reasonably reproduce the key features of the PG structure.

The inspection of the calculated binding energies E_b (see Table 2) shows that AIREBO-M is the most accurate potential in describing the relative stability of PG and the only potential which returned E_b accurate to no less than 0.1 eV/atom. However, three other potentials, namely T05, REAX05 and REAX08, provided an acceptable result, which differed from the *ab initio* one by no more than 30%. On the other hand, three potentials – namely SW, ISW and MEAM – failed in capturing the penta-graphene stability, yielding negative values of E_b and predicting PG to be more stable than graphene, which is an unacceptable result.

We note that for all the considered REAX potentials we also localized other local minima. All of them were found to lie far from the global minimum, with the energy distance greater than 0.1 eV/atom. For the sake of completeness in Table 4 we provide detailed information regarding the structure of this highly-lying minima. Since none of the existing *ab initio* studies has reported similar observation we have performed an additional DFT calculations [68–70], using a formalism analogous to

Potential	a (Å)	h (Å)	d_1 (Å)	d_2 (Å)	θ_1 (degrees)	θ_2 (degrees)	E_b (eV/atom)
REAX05	3.625	0.674	1.600	1.199	100.2	130.2	1.272
	3.713	0.826	1.636	1.584	104.8	119.3	1.507
REAX08	3.697	0.546	1.554	1.336	97.1	138.8	1.077
	3.570	0.710	1.594	1.192	101.5	127.1	1.199
REAX15	3.731	0.805	1.632	1.587	104.1	120.9	1.201

Table 4: Other (non-global) minima located for REAX potentials.

that of Zhang *et al.* [9]. These calculations have shown that the additional minima identified are just an artifact introduced by the REAX formalism, as they were not confirmed as minima in DFT calculations. We note that this feature (ie. the existence of many PG-like minima) was not recognized for the other potentials, all of which returned a single, well-defined minimum.

Now we move to the presentation of the calculated mechanical properties, summarized in Table 3. We focus on the not-yet-rejected potentials (*i.e.*: T89, T05, REAX05, REAX08, REAX15, LCBOP and ABOP) and skip the discussion of the results obtained for the other potentials, presenting them only for the sake of completeness.

All parameterizations of the REAX force field have failed in predicting the auxeticity of PG, providing Poisson's ratio which is positive and – what is especially important – often very high. For the REAX08 potential the obtained value ($\nu = 0.493$), almost corresponds to a perfectly incompressible material (which has $\nu = 0.5$ – the maximum possible value), which is a completely unacceptable result. A similar value was obtained for the REAX05 parameterization.

The remaining four potentials (T89, T05, LCBOP and ABOP) correctly render PG to be auxetic, returning a negative Poisson's ratio. However, for one of them, namely T89, the agreement with the *ab initio* result is very poor. Despite the fact that the T89 potential almost perfectly reproduces C_{66}, it strongly underestimates two other elastic constants, by 20% (C_{11}) and 104% (C_{12}). As a result, the mechanical moduli are mispredicted by more than 20% (the Young's modulus) and 150%

(the Poisson's ratio). The latter failure makes this potential unacceptable when investigating the auxetic properties of PG.

Among the remaining three potentials the T05 potential gave the best results, with only slightly underestimated the C_{11} (8% relative error) and C_{12} (15%) elastic constants. The C_{66} elastic constant is also quite well reproduced, with the relative error smaller than 7%.

The other two potentials are less accurate. The LCBOP potential, despite its ability to reproduce the C_{11} elastic constant (with 11% relative error), significantly overestimates the C_{12} and C_{66} elastic constants, with the corresponding relative errors being as high as 40%. In the case of the ABOP potential the C_{11} and C_{12} elastic constants are significantly mispredicted, with the very low ($\approx 2\%$) error recorded for the Poisson's ratio, being just a coincidence of the overestimated C_{11} constant and the underestimated C_{12} constant, both by $\approx 20\%$.

In light of the above presented analysis, we conclude that the T05 potential should be the potential of choice when taking the mechanical properties as the main indicator of the potential's quality. To emphasize its overall success, we stress that this potential not only correctly reproduces the mechanical properties of PG, but also yields the structural properties which are within the acceptance limits, typically used for the empirical potentials.

3.3. Further tests

In the two previous subsections we have shown that the T05 potential correctly captures all important features of a PG structure and accurately reproduces its linear (*i.e.* low deformation) mechanical response. In order to check if the T05 potential is also able to reproduce the non-linear mechanical behavior of PG, we performed additional tests comparing stress–strain dependencies for the equibiaxial stretching (deformation D_1, with $\varepsilon_1 = \varepsilon_2 = x$) and large deformations ($x \in [0, 0.30]$). In Figure 3 we present the results obtained for the T05 potential and compare it against the *ab initio* result of Ref. [9]. We also present the results obtained for the REAX05, REAX08, and ABOP potentials, in order to illustrate further deficiencies of these approaches.

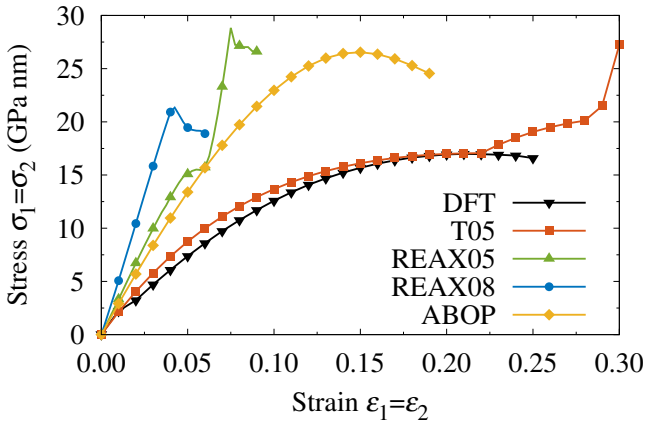

Figure 3: Stress–strain relationships calculated for T05, REAX05, REAX08 and ABOP potentials, compared with the *ab initio* result of Zhang *et al.* [9].

Even a first glance shows that the ABOP potential is unable to reproduce the large strain behavior of PG, which is evidenced by the drastic differences seen in the stress–strain dependencies. It also fails in predicting the strength of PG, which according to it breaks at $x \approx 0.18$.

Similarly, both the REAX potentials considered here are also unable to correctly describe the mechanical response of PG. For these two potentials we identified another important failure. We noticed that even at relatively small deformations (at $x \approx 0.075$ and $x \approx 0.04$, for the REAX05 and REAX08 potentials, respectively) the simulated system started to display some strange behavior which was accompanied by a transformation of the PG structure into some other – similar but less-ordered – form, with several d_1 and d_2 distances present. We recognize this behavior as an artifact introduced by the REAX approach, which is another argument for not using this model. This observation clearly shows that the REAX approach runs into significant difficulties when it comes to the modeling of carbon forms with strongly elongated bonds. At the same time, it suggests that the results presented by Cranford in Ref. [18] regarding PG instability may be incorrect, because of the inadequacy of the REAX potential.

In contrast to the previous three potentials, T05 gives results which are in a reasonable agreement with the *ab initio* calculations, up to strains as high as $x = 0.22$.

We found that the change in the slope visible above this value should be attributed to the fact, that at this strain the interlayer spacing h reaches the zero value. As a result, the mechanism of deformation changes, from quasi-two-dimensional to purely two-dimensional, resulting in the stiffening of PG. The second change of the slope, which occurs at $x = 0.28$, originates from the fact, that at this point the T05 potential automatically switches its functional form. This was confirmed by a detailed examination of the atomic configurations, which showed that at $x = 0.28$ the bond length d_1 reached the value 1.85 Å, which is the lower cutoff radius of the cutoff function used in the T05 potential (compare with $D - R$ of Ref. [39]).

To conclude, despite the fact that the T05 potential does not reproduce the DFT results above $x = 0.22$, we believe that the general good agreement obtained here not only further motivates its choice, but also justifies its potential use in studies on the non-linear mechanical behavior of PG.

4. Molecular Dynamics simulations

4.1. Simulation protocol

In order to test if the chosen T05 potential is able to reproduce the finite-temperature behavior of PG we performed a series of molecular dynamics simulations. The main scope here was to test how the temperature and the stresses influence the stability of PG described with the T05 potential, and if the obtained picture is consistent with the *ab initio* studies of Ref. [9].

Our detailed protocol was as follows. The structure optimized for 0 K was first equilibrated at the desired temperature T, by running a NpT simulation at zero pressure, during which the equilibrium system size was determined. This was followed by a series of NVT simulations, in which the mechanical response of PG was investigated by applying equibiaxial stretching (deformation D_1, with $\varepsilon_1 = \varepsilon_2 = x$). We considered eight different temperatures $T = 150, 300, \ldots, 1200$ K, and studied strains ranging from $x = 0$ to $x = 0.40$, with the increment $\Delta x = 0.001$.

For each studied temperature the entire process carried out consisted of a series of continued simulations, where the final state obtained for the strain x was used as an initial condition in a simulation performed for the strain $x + \Delta x$. In each

simulation the system was first equilibrated for 50 000 steps, which was followed by sampling over 200 000 steps. The equations of motion were integrated using the velocity Verlet algorithm [71] with the timestep $\Delta t = 0.5$ fs. The temperature and pressure were controlled using Nose-Hoover thermostat [72, 73] and Parinello-Rahman barostat [74], as implemented in the LAMMPS program [67, 75]. Similarly to the MS simulations, the simulated system consisted of 600 atoms and PBCs were applied along x and y directions.

The entire process was repeated for 5 times in order to test how the initial condition influenced the results. This was achieved by restarting the entire process with different randomly generated initial velocities. All the characteristics presented later were obtained by averaging over these independent, uncorrelated runs.

Having performed the simulations we examined the stability of PG. This was achieved by analyzing configurations collected during the MD simulations, which were stored every 200 steps. For each of the 5 independent runs we determined the critical strain ε_c, at which permanent bond breaking started to occur.

4.2. Results

In Figure 4 we present the run average critical strain ε_c, together with its standard deviation. At low temperatures (*i.e.* below 300 K) PG displays very high stability, being able to sustain strains higher than 30%. Above 300 K a significant decrease in the stability is observed. As a result at 750 K the equibiaxial breaking strain reaches $\approx 10\%$. Above this point the critical strain decreases linearly with the temperature. This clear tendency allowed us to estimate the critical temperature, *i.e.* the temperature at which PG breaks at zero strain, which by linear extrapolation was found to be 1270 K. This result is in a good accordance with Ref. [9], which reported that PG is stable up to temperatures as high as 1000 K. We note that it is impossible to present a more detailed comparison because there is no relevant *ab initio* data available. It is worth pointing out that in all cases we found out that the failure of PG was due to the breaking of (longer) C1-C2 bonds. This result is consistent with more recent *ab initio* calculations of Sun *et al.* [11].

The performed MD simulations allowed us to study the in-plane (xy) and out-

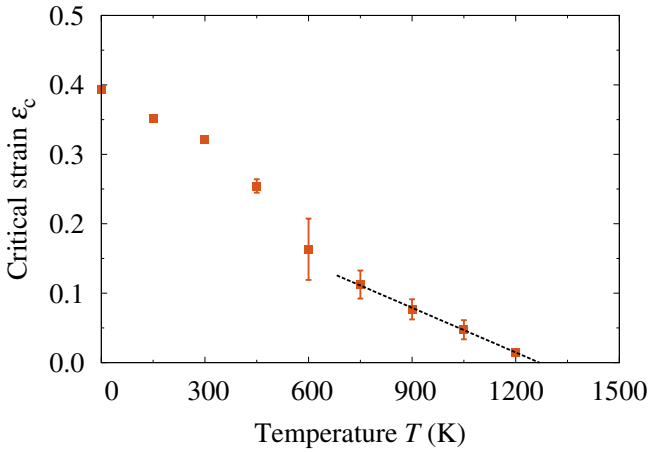

Figure 4: Stability of penta-graphene described with the T05 potential. Error bars represent one standard deviation. The dashed line represents the linear fit obtained for $T \geq 750$ K.

of-plane (z) thermal expansion of PG. For this purpose we checked how the lattice parameter a and interlayer spacing h depend on the temperature T. The latter was calculated by using the formula:

$$h = \frac{\langle z_{\mathrm{upp}} \rangle - \langle z_{\mathrm{low}} \rangle}{2}. \tag{7}$$

Here, $\langle z_{\mathrm{lay}} \rangle$ denotes the average z-component of position calculated for atoms belonging to the upper ($\langle z_{\mathrm{upp}} \rangle$), middle ($\langle z_{\mathrm{mid}} \rangle$) and lower ($\langle z_{\mathrm{low}} \rangle$) layers, respectively. For the three considered quantities we also calculated standard deviations of the mean value, which will be denoted by $\sigma(z_{\mathrm{upp}})$, $\sigma(z_{\mathrm{mid}})$ and $\sigma(z_{\mathrm{low}})$, respectively. We found that $\langle z_{\mathrm{upp}} \rangle \approx -\langle z_{\mathrm{low}} \rangle$ and $\langle z_{\mathrm{mid}} \rangle \approx 0$, noting also that $\sigma(z_{\mathrm{upp}}) \approx \sigma(z_{\mathrm{mid}}) \approx \sigma(z_{\mathrm{low}})$.

In Figure 5a we present the temperature dependence of the lattice parameter a (red squares) and the interlayer spacing h (blue circles). Both the considered characteristics are clearly linear in the entire temperature range studied. By linear fitting, we estimated two coefficients of thermal expansion (CTE). For the in-plane direction we obtained $\alpha_{xy} = 6.3 \times 10^{-6}$ K^{-1}. For the out-of-plane direction we obtained $\alpha_z = -4.8 \times 10^{-6}$ K^{-1}. The negative value indicates that the two outer layers move closer to each other when the temperature is increased. However, this result should not be considered as an indication of anomalous behavior (*i.e.* negative

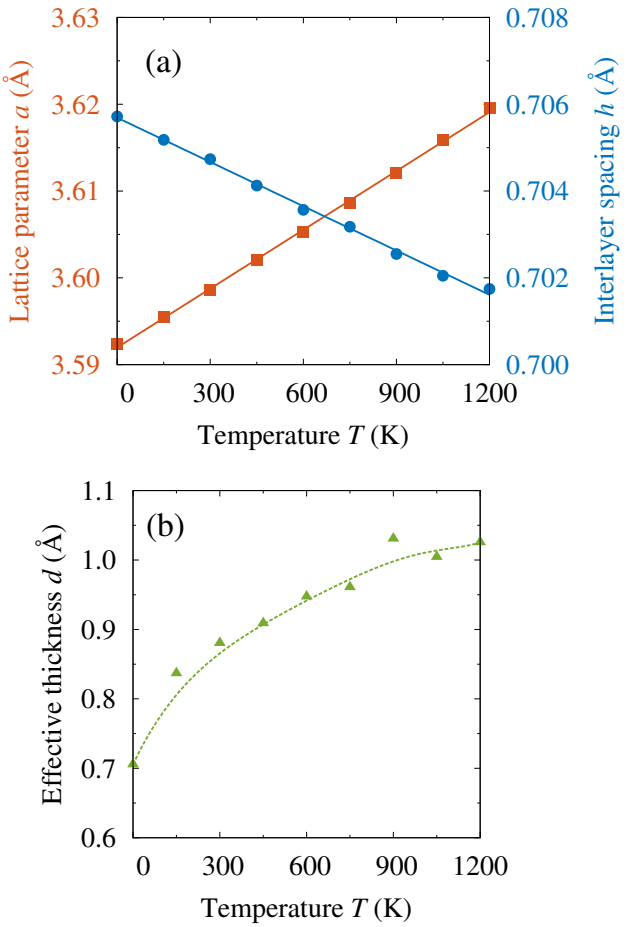

Figure 5: Thermal expansion of penta-graphene described with T05 potential. The solid lines on panel a represent linear fits, while the dashed line on panel b serves as a guide for the eye.

thermal expansion), since the h parameter is unable to capture the real change in the PG thickness.

The increase in amplitude of the out-of-plane vibrations can be easily accounted for with the aid of the following quantity:

$$d = h + \frac{\sigma(z_{\mathrm{upp}}) + \sigma(z_{\mathrm{low}})}{2}, \tag{8}$$

which measures the effective thickness of PG. The calculated temperature dependence of d is presented in Figure 5b. It is clearly visible that PG exhibits positive and non-linear thermal expansion in the z direction. To show how significant it is, we note that between 0 K and 1200 K the thickness of PG increases by more than 40%, which implies that the corresponding CTE is of the order of 10^{-4} K^{-1}.

Despite the fact that the temperature has a considerable influence on the stability of PG, we found that it only slightly alters its in-plane stiffness. This can be very easily seen by looking at the stress-strain curves (Fig. 6).

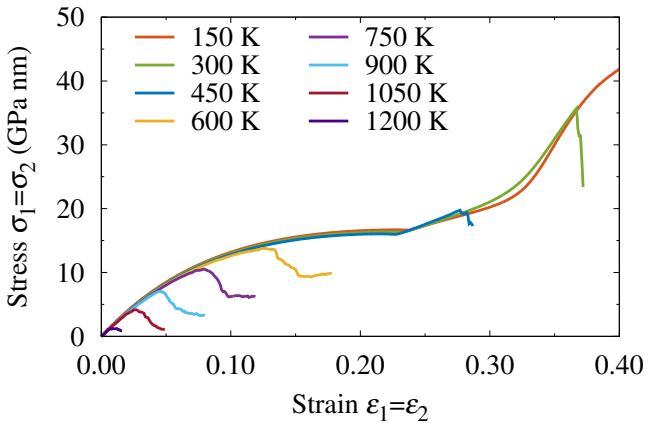

Figure 6: Finite-temperature mechanical response of penta-graphene described with the T05 potential. The presented stress-strain curves correspond to the equibiaxial stretching.

5. Summary

We performed a careful validation of the interatomic potentials available for elemental carbon, with the scope to choose the potential suitable for the modeling of penta-graphene. We considered 14 different empirical potentials, *i.a.*, three Tersoff-type potentials, two Stillinger-Weber-type potentials, three REBO models, and three parameterizations of the REAX force field.

By using molecular statics method we calculated the properties of PG at 0 K. By comparing the obtained results with the available *ab initio* data we demonstrated that there is only one potential, which is able to correctly describe PG, namely the Tersoff-type potential proposed by Erhart and Albe in 2005 [39]. We showed that this potential gives structural, mechanical and energetic parameters which are in accordance with the *ab initio* studies. We also demonstrated that this potential correctly reproduces the large strain behavior of PG, which makes it suitable for *e.g.* studying auxetic properties of PG.

In order to check if the chosen potential correctly reproduces the finite-temperature behavior of PG, we performed a series of molecular dynamics simulations. We found that PG described with the chosen potential is stable up to temperatures as high as 1260 K, which also agrees with the *ab initio* calculations.

Acknowledgements

We acknowledge the support of the Polish Ministry of Science and Higher Education (Grant IP2012 043972) and the TASK Academic Computer Centre (Gdańsk, Poland). This research was also supported in part by the PL-Grid Infrastructure (Grant POIG.02.03.00-00-096/10).

References

[1] S. Iijima, Helical microtubules of graphitic carbon, Nature 354 (1991) 56 – 58. doi:10.1038/354056a0.

[2] T. W. Ebbesen, P. M. Ajayan, Large-scale synthesis of carbon nanotubes, Nature 358 (1992) 220 – 222. doi:10.1038/358220a0.

[3] C. Berger, Z. Song, T. Li, X. Li, A. Y. Ogbazghi, R. Feng, et al., Ultrathin epitaxial graphite: 2d electron gas properties and a route toward graphene-based nanoelectronics, The Journal of Physical Chemistry B 108 (52) (2004) 19912 – 19916. arXiv:http://dx.doi.org/10.1021/jp040650f, doi:10.1021/jp040650f.
URL http://dx.doi.org/10.1021/jp040650f

[4] K. S. Novoselov, A. K. Geim, S. V. Morozov, D. Jiang, Y. Zhang, S. V. Dubonos, et al., Electric field effect in atomically thin carbon films, Science 306 (5696) (2004) 666–669. arXiv:http://science.sciencemag.org/content/306/5696/666.full.pdf, doi:10.1126/science.1102896.
URL http://science.sciencemag.org/content/306/5696/666

[5] C. Su, H. Jiang, J. Feng, Two-dimensional carbon allotrope with strong electronic anisotropy, Phys. Rev. B 87 (2013) 075453. doi:10.1103/PhysRevB.87.075453.
URL http://link.aps.org/doi/10.1103/PhysRevB.87.075453

[6] W.-J. Yin, Y.-E. Xie, L.-M. Liu, R.-Z. Wang, X.-L. Wei, L. Lau, et al., R-graphyne: a new two-dimensional carbon allotrope with versatile dirac-like point in nanoribbons, J. Mater. Chem. A 1 (2013) 5341–5346. doi:10.1039/C3TA00097D.
URL http://dx.doi.org/10.1039/C3TA00097D

[7] B. R. Sharma, A. Manjanath, A. K. Singh, pentahexoctite: A new two-dimensional allotrope of carbon, Scientific Reports 4 (2014) 7164. doi:http://dx.doi.org/10.1038/srep07164.

[8] Z. Wang, X.-F. Zhou, X. Zhang, Q. Zhu, H. Dong, M. Zhao, et al., Phagraphene: A low-energy graphene allotrope composed of 5-6-7 carbon rings with distorted dirac cones, Nano Letters 15 (9) (2015) 6182–6186, pMID: 26262429. arXiv:http://dx.doi.org/10.1021/acs.nanolett.5b02512, doi:10.1021/acs.nanolett.5b02512.
URL http://dx.doi.org/10.1021/acs.nanolett.5b02512

[9] S. Zhang, J. Zhou, Q. Wang, X. Chen, Y. Kawazoe, P. Jena, Penta-graphene: A new carbon allotrope, Proceedings of the National Academy of Sciences 112 (8) (2015) 2372–2377. arXiv:http://www.pnas.org/content/112/8/2372.full.pdf, doi:10.1073/pnas.1416591112.
URL http://www.pnas.org/content/112/8/2372.abstract

[10] X. Zhang, L. Wei, J. Tan, M. Zhao, Prediction of an ultrasoft graphene allotrope with dirac cones, Carbon 105 (2016) 323 – 329. doi:http://dx.doi.org/10.1016/j.carbon.2016.04.058.
URL http://www.sciencedirect.com/science/article/pii/S0008622316303293

[11] H. Sun, S. Mukherjee, C. V. Singh, Mechanical properties of monolayer penta-graphene and phagraphene: a first-principles study, Phys. Chem. Chem. Phys. 18 (2016) 26736–26742. doi:10.1039/C6CP04595B.
URL http://dx.doi.org/10.1039/C6CP04595B

[12] Z. Zhao, F. Tian, X. Dong, Q. Li, Q. Wang, H. Wang, et al., Tetragonal allotrope of group 14 elements, Journal of the American Chemical Society 134 (30) (2012) 12362–12365, pMID: 22803841. arXiv:http://dx.doi.org/10.1021/ja304380p, doi:10.1021/ja304380p.
URL http://dx.doi.org/10.1021/ja304380p

[13] X. Jiang, C. Århammar, P. Liu, J. Zhao, R. Ahuja, The r3-carbon allotrope: a pathway towards glassy carbon under high pressure, Scientific Reports 3 (2013) 1877. doi:http://dx.doi.org/10.1038/srep01877.

[14] N. U. Zhanpeisov, Theoretical dft study on structure and chemical activity of new carbon k4 clusters, Research on Chemical Intermediates 39 (5) (2013) 2141–2148. doi:10.1007/s11164-012-0746-z.
URL http://dx.doi.org/10.1007/s11164-012-0746-z

[15] S. Zhang, Q. Wang, X. Chen, P. Jena, Stable three-dimensional metallic carbon with interlocking hexagons, Proceedings of the National Academy of Sciences 110 (47) (2013) 18809–18813. arXiv:http://www.pnas.org/content/110/47/18809.full.pdf, doi:10.1073/pnas.1311028110.
URL http://www.pnas.org/content/110/47/18809.abstract

[16] L. A. Burchfield, M. A. Fahim, R. S. Wittman, F. Delodovici, N. Manini, Novamene: A new class of carbon allotropes, Heliyon 3 (2) (2017) Article e00242. doi:http://dx.doi.org/10.1016/j.heliyon.2017.e00242.
URL http://www.sciencedirect.com/science/article/pii/S2405844016310386

[17] C. P. Ewels, X. Rocquefelte, H. W. Kroto, M. J. Rayson, P. R. Briddon, M. I. Heggie, Predicting experimentally stable allotropes: Instability of penta-graphene, Proceedings of the National Academy of Sciences 112 (51) (2015) 15609–15612. arXiv:http://www.pnas.org/content/112/51/15609.full.pdf, doi:10.1073/pnas.1520402112.
URL http://www.pnas.org/content/112/51/15609.abstract

[18] S. W. Cranford, When is 6 less than 5? penta- to hexa-graphene transition, Carbon 96 (2016) 421 – 428. doi:http://dx.doi.org/10.1016/j.carbon.2015.09.092.
URL http://www.sciencedirect.com/science/article/pii/S0008622315303109

[19] G. R. Berdiyorov, G. Dixit, M. E. Madjet, Band gap engineering in penta-graphene by substitutional doping: first-principles calculations, Journal of

Physics: Condensed Matter 28 (47) (2016) 475001.
URL http://stacks.iop.org/0953-8984/28/i=47/a=475001

[20] X. Li, S. Zhang, F. Q. Wang, Y. Guo, J. Liu, Q. Wang, Tuning the electronic and mechanical properties of penta-graphene via hydrogenation and fluorination, Phys. Chem. Chem. Phys. 18 (2016) 14191–14197. doi:10.1039/C6CP01092J.
URL http://dx.doi.org/10.1039/C6CP01092J

[21] W. Xu, G. Zhang, B. Li, Thermal conductivity of penta-graphene from molecular dynamics study, The Journal of Chemical Physics 143 (15) (2015) 154703. doi:http://dx.doi.org/10.1063/1.4933311.
URL http://scitation.aip.org/content/aip/journal/jcp/143/15/10.1063/1.4933311

[22] X. Wu, V. Varshney, J. Lee, T. Zhang, J. L. Wohlwend, A. K. Roy, et al., Hydrogenation of penta-graphene leads to unexpected large improvement in thermal conductivity, Nano Letters 16 (6) (2016) 3925–3935, pMID: 27152879. arXiv:http://dx.doi.org/10.1021/acs.nanolett.6b01536, doi:10.1021/acs.nanolett.6b01536.
URL http://dx.doi.org/10.1021/acs.nanolett.6b01536

[23] Z. G. Yu, Y.-W. Zhang, A comparative density functional study on electrical properties of layered penta-graphene, Journal of Applied Physics 118 (16) (2015) 165706. arXiv:http://dx.doi.org/10.1063/1.4934855, doi:10.1063/1.4934855.
URL http://dx.doi.org/10.1063/1.4934855

[24] B. Rajbanshi, S. Sarkar, B. Mandal, P. Sarkar, Energetic and electronic structure of penta-graphene nanoribbons, Carbon 100 (2016) 118 – 125. doi:http://dx.doi.org/10.1016/j.carbon.2016.01.014.
URL http://www.sciencedirect.com/science/article/pii/S0008622316300148

[25] B. Xiao, Y.-c. Li, X.-f. Yu, J.-b. Cheng, Penta-graphene: A promising anode material as the li/na-ion battery with both extremely high theoretical capacity and fast charge discharge rate, ACS Applied Materials & Interfaces 8 (51) (2016) 35342–35352, pMID: 27977126. arXiv:http://dx.doi.org/10.1021/acsami.6b12727, doi:10.1021/acsami.6b12727.
URL http://dx.doi.org/10.1021/acsami.6b12727

[26] S. Ebrahimi, Effect of hydrogen coverage on the buckling of penta-graphene by molecular dynamics simulation, Molecular Simulation 42 (17) (2016) 1485–1489. arXiv:http://dx.doi.org/10.1080/08927022.2016.1205191, doi:10.1080/08927022.2016.1205191.
URL http://dx.doi.org/10.1080/08927022.2016.1205191

[27] P. Avramov, V. Demin, M. Luo, C. H. Choi, P. B. Sorokin, B. Yakobson, et al., Translation symmetry breakdown in low-dimensional lattices of pentagonal rings, The Journal of Physical Chemistry Letters 6 (22) (2015) 4525–4531, pMID: 26582476. arXiv:http://dx.doi.org/10.1021/acs.jpclett.5b02309, doi:10.1021/acs.jpclett.5b02309.
URL http://dx.doi.org/10.1021/acs.jpclett.5b02309

[28] T. Stauber, J. I. Beltrán, J. Schliemann, Tight-binding approach to penta-graphene, Scientific Reports 6 (2016) 22672. doi:10.1038/srep22672.
URL http://dx.doi.org/10.1038/srep22672

[29] O. Rahaman, B. Mortazavi, A. Dianat, G. Cuniberti, T. Rabczuk, Metamorphosis in carbon network: From penta-graphene to biphenylene under uniaxial tension, FlatChem 1 (2017) 65 – 73. doi:http://dx.doi.org/10.1016/j.flatc.2016.12.001.
URL http://www.sciencedirect.com/science/article/pii/S2452262716300526

[30] X. Wei, B. Fragneaud, C. A. Marianetti, J. W. Kysar, Nonlinear elastic behavior of graphene: *Ab initio* calculations to continuum description, Phys. Rev. B

80 (2009) 205407. doi:10.1103/PhysRevB.80.205407.
URL http://link.aps.org/doi/10.1103/PhysRevB.80.205407

[31] E. Pop, V. Varshney, A. K. Roy, Thermal properties of graphene: Fundamentals and applications, MRS Bulletin 37 (12) (2012) 1273–1281. doi:https://doi.org/10.1557/mrs.2012.203.

[32] K. Chenoweth, A. C. T. van Duin, W. A. Goddard, Reaxff reactive force field for molecular dynamics simulations of hydrocarbon oxidation, The Journal of Physical Chemistry A 112 (5) (2008) 1040–1053. arXiv:http://dx.doi.org/10.1021/jp709896w, doi:10.1021/jp709896w.
URL http://dx.doi.org/10.1021/jp709896w

[33] D. W. Brenner, O. A. Shenderova, J. A. Harrison, S. J. Stuart, B. Ni, S. B. Sinnott, A second-generation reactive empirical bond order (rebo) potential energy expression for hydrocarbons, Journal of Physics: Condensed Matter 14 (4) (2002) 783.
URL http://stacks.iop.org/0953-8984/14/i=4/a=312

[34] J. Tersoff, Modeling solid-state chemistry: Interatomic potentials for multicomponent systems, Phys. Rev. B 39 (1989) 5566–5568. doi:10.1103/PhysRevB.39.5566.
URL http://link.aps.org/doi/10.1103/PhysRevB.39.5566

[35] J. Tersoff, Erratum: Modeling solid-state chemistry: Interatomic potentials for multicomponent systems, Phys. Rev. B 41 (1990) 3248–3248. doi:10.1103/PhysRevB.41.3248.2.
URL http://link.aps.org/doi/10.1103/PhysRevB.41.3248.2

[36] L. Lindsay, D. A. Broido, Optimized tersoff and brenner empirical potential parameters for lattice dynamics and phonon thermal transport in carbon nanotubes and graphene, Phys. Rev. B 81 (2010) 205441. doi:10.1103/PhysRevB.81.205441.
URL http://link.aps.org/doi/10.1103/PhysRevB.81.205441

[37] L. Lindsay, D. A. Broido, Erratum: Optimized tersoff and brenner empirical potential parameters for lattice dynamics and phonon thermal transport in carbon nanotubes and graphene [phys. rev. b **81**, 205441 (2010)], Phys. Rev. B 82 (2010) 209903. doi:10.1103/PhysRevB.82.209903.
URL http://link.aps.org/doi/10.1103/PhysRevB.82.209903

[38] N. Marks, Modelling diamond-like carbon with the environment-dependent interaction potential, Journal of Physics: Condensed Matter 14 (11) (2002) 2901.
URL http://stacks.iop.org/0953-8984/14/i=11/a=308

[39] P. Erhart, K. Albe, Analytical potential for atomistic simulations of silicon, carbon, and silicon carbide, Phys. Rev. B 71 (2005) 035211. doi:10.1103/PhysRevB.71.035211.
URL http://link.aps.org/doi/10.1103/PhysRevB.71.035211

[40] P. Mahon, B. A. Pailthorpe, G. B. Bacskay, A quantum mechanical calculation of interatomic interactions in diamond, Philosophical Magazine Part B 63 (6) (1991) 1419–1430. arXiv:http://dx.doi.org/10.1080/13642819108205571, doi:10.1080/13642819108205571.
URL http://dx.doi.org/10.1080/13642819108205571

[41] A. S. Barnard, S. P. Russo, Development of an improved stillinger-weber potential for tetrahedral carbon using ab initio (hartree-fock and mp2) methods, Molecular Physics 100 (10) (2002) 1517–1525. arXiv:http://dx.doi.org/10.1080/00268970110109853, doi:10.1080/00268970110109853.
URL http://dx.doi.org/10.1080/00268970110109853

[42] D. W. Brenner, Empirical potential for hydrocarbons for use in simulating the chemical vapor deposition of diamond films, Phys. Rev. B 42 (1990) 9458–9471. doi:10.1103/PhysRevB.42.9458.
URL http://link.aps.org/doi/10.1103/PhysRevB.42.9458

[43] D. W. Brenner, Erratum: Empirical potential for hydrocarbons for use in simulating the chemical vapor deposition of diamond films, Phys. Rev. B 46 (1992) 1948–1948. doi:10.1103/PhysRevB.46.1948.2.
URL http://link.aps.org/doi/10.1103/PhysRevB.46.1948.2

[44] S. J. Stuart, A. B. Tutein, J. A. Harrison, A reactive potential for hydrocarbons with intermolecular interactions, The Journal of Chemical Physics 112 (14) (2000) 6472–6486. doi:http://dx.doi.org/10.1063/1.481208.
URL http://scitation.aip.org/content/aip/journal/jcp/112/14/10.1063/1.481208

[45] T. C. O'Connor, J. Andzelm, M. O. Robbins, Airebo-m: A reactive model for hydrocarbons at extreme pressures, The Journal of Chemical Physics 142 (2) (2015) 024903. arXiv:http://dx.doi.org/10.1063/1.4905549, doi:10.1063/1.4905549.
URL http://dx.doi.org/10.1063/1.4905549

[46] A. C. T. van Duin, S. Dasgupta, F. Lorant, W. A. Goddard, Reaxff: A reactive force field for hydrocarbons, The Journal of Physical Chemistry A 105 (41) (2001) 9396–9409. arXiv:http://dx.doi.org/10.1021/jp004368u, doi:10.1021/jp004368u.
URL http://dx.doi.org/10.1021/jp004368u

[47] K. D. Nielson, A. C. T. van Duin, J. Oxgaard, W.-Q. Deng, W. A. Goddard, Development of the reaxff reactive force field for describing transition metal catalyzed reactions, with application to the initial stages of the catalytic formation of carbon nanotubes, The Journal of Physical Chemistry A 109 (3) (2005) 493–499, pMID: 16833370. arXiv:http://dx.doi.org/10.1021/jp046244d, doi:10.1021/jp046244d.
URL http://dx.doi.org/10.1021/jp046244d

[48] S. G. Srinivasan, A. C. T. van Duin, P. Ganesh, Development of a reaxff potential for carbon condensed phases and its application to the thermal fragmentation of a large fullerene, The Journal of Physical Chemistry A 119 (4)

(2015) 571–580, pMID: 25562718. arXiv:http://dx.doi.org/10.1021/jp510274e, doi:10.1021/jp510274e.
URL http://dx.doi.org/10.1021/jp510274e

[49] M. I. Baskes, Modified embedded-atom potentials for cubic materials and impurities, Phys. Rev. B 46 (1992) 2727–2742. doi:10.1103/PhysRevB.46.2727.
URL http://link.aps.org/doi/10.1103/PhysRevB.46.2727

[50] J. H. Los, A. Fasolino, Intrinsic long-range bond-order potential for carbon: Performance in monte carlo simulations of graphitization, Phys. Rev. B 68 (2003) 024107. doi:10.1103/PhysRevB.68.024107.
URL http://link.aps.org/doi/10.1103/PhysRevB.68.024107

[51] X. W. Zhou, D. K. Ward, M. E. Foster, An analytical bond-order potential for carbon, Journal of Computational Chemistry 36 (23) (2015) 1719–1735. doi:10.1002/jcc.23949.
URL http://dx.doi.org/10.1002/jcc.23949

[52] N. A. Marks, Generalizing the environment-dependent interaction potential for carbon, Phys. Rev. B 63 (2000) 035401. doi:10.1103/PhysRevB.63.035401.
URL http://link.aps.org/doi/10.1103/PhysRevB.63.035401

[53] A. Stukowski, Visualization and analysis of atomistic simulation data with ovito - the open visualization tool, Modelling and Simulation in Materials Science and Engineering 18 (1) (2010) 015012.
URL http://stacks.iop.org/0965-0393/18/i=1/a=015012

[54] J. Tersoff, Empirical interatomic potential for silicon with improved elastic properties, Phys. Rev. B 38 (1988) 9902–9905. doi:10.1103/PhysRevB.38.9902.
URL http://link.aps.org/doi/10.1103/PhysRevB.38.9902

[55] F. H. Stillinger, T. A. Weber, Computer simulation of local order in condensed phases of silicon, Phys. Rev. B 31 (1985) 5262–5271. doi:10.1103/PhysRevB.31.5262.
URL http://link.aps.org/doi/10.1103/PhysRevB.31.5262

[56] F. H. Stillinger, T. A. Weber, Erratum: Computer simulation of local order in condensed phases of silicon [phys. rev. b 31, 5262 (1985)], Phys. Rev. B 33 (1986) 1451–1451. doi:10.1103/PhysRevB.33.1451.
URL http://link.aps.org/doi/10.1103/PhysRevB.33.1451

[57] A. Strachan, A. C. T. van Duin, D. Chakraborty, S. Dasgupta, W. A. Goddard, Shock waves in high-energy materials: The initial chemical events in nitramine rdx, Phys. Rev. Lett. 91 (2003) 098301. doi:10.1103/PhysRevLett.91.098301.
URL http://link.aps.org/doi/10.1103/PhysRevLett.91.098301

[58] J. Budzien, A. P. Thompson, S. V. Zybin, Reactive molecular dynamics simulations of shock through a single crystal of pentaerythritol tetranitrate, The Journal of Physical Chemistry B 113 (40) (2009) 13142–13151. arXiv:http://dx.doi.org/10.1021/jp9016695, doi:10.1021/jp9016695.
URL http://dx.doi.org/10.1021/jp9016695

[59] M. Aryanpour, A. C. T. van Duin, J. D. Kubicki, Development of a reactive force field for iron-oxyhydroxide systems, The Journal of Physical Chemistry A 114 (21) (2010) 6298–6307. arXiv:http://dx.doi.org/10.1021/jp101332k, doi:10.1021/jp101332k.
URL http://dx.doi.org/10.1021/jp101332k

[60] T. R. Mattsson, J. M. D. Lane, K. R. Cochrane, M. P. Desjarlais, A. P. Thompson, F. Pierce, et al., First-principles and classical molecular dynamics simulation of shocked polymers, Phys. Rev. B 81 (2010) 054103. doi:10.1103/PhysRevB.81.054103.
URL http://link.aps.org/doi/10.1103/PhysRevB.81.054103

[61] L. Liu, Y. Liu, S. V. Zybin, H. Sun, W. A. Goddard, Reaxff-lg: Correction of the reaxff reactive force field for london dispersion, with applications to the equations of state for energetic materials, The Journal of Physical Chemistry A 115 (40) (2011) 11016–11022. arXiv:http://dx.doi.org/10.1021/jp201599t, doi:10.1021/jp201599t.
URL http://dx.doi.org/10.1021/jp201599t

[62] S. K. Singh, S. G. Srinivasan, M. Neek-Amal, S. Costamagna, A. C. T. van Duin, F. M. Peeters, Thermal properties of fluorinated graphene, Phys. Rev. B 87 (2013) 104114. doi:10.1103/PhysRevB.87.104114.
URL http://link.aps.org/doi/10.1103/PhysRevB.87.104114

[63] T. P. Senftle, S. Hong, M. M. Islam, S. B. Kylasa, Y. Zheng, Y. K. Shin, et al., The reaxff reactive force-field: development, applications and future directions, Npj Computational Materials 2. doi:10.1038/npjcompumats.2015.11.
URL http://dx.doi.org/10.1038/npjcompumats.2015.11

[64] C. A. Coulson, The electronic structure of some polyenes and aromatic molecules. vii. bonds of fractional order by the molecular orbital method, Proceedings of the Royal Society of London A: Mathematical, Physical and Engineering Sciences 169 (938) (1939) 413–428. arXiv:http://rspa.royalsocietypublishing.org/content/169/938/413.full.pdf, doi:10.1098/rspa.1939.0006.
URL http://rspa.royalsocietypublishing.org/content/169/938/413

[65] J. Tersoff, New empirical model for the structural properties of silicon, Phys. Rev. Lett. 56 (1986) 632–635. doi:10.1103/PhysRevLett.56.632.
URL http://link.aps.org/doi/10.1103/PhysRevLett.56.632

[66] E. Polak, G. Ribiére, Note sur la convergence de méthodes de directions conjuguées, ESAIM: Mathematical Modelling and Numerical Analysis - Modélisation Mathématique et Analyse Numérique 3 (R1) (1969) 35–43.
URL http://eudml.org/doc/193115

[67] S. Plimpton, Fast parallel algorithms for short-range molecular dynamics, Journal of Computational Physics 117 (1) (1995) 1 – 19. doi:http://dx.doi.org/10.1006/jcph.1995.1039.
URL http://www.sciencedirect.com/science/article/pii/S002199918571039X

[68] C.-K. Skylaris, P. D. Haynes, A. A. Mostofi, M. C. Payne, Introducing

ONETEP: Linear-scaling density functional simulations on parallel computers, J. Chem. Phys. 122 (2005) 084119.

[69] N. D. M. Hine, M. Robinson, P. D. Haynes, C.-K. Skylaris, M. C. Payne, A. A. Mostofi, Accurate ionic forces and geometry optimization in linear-scaling density-functional theory with local orbitals, Phys. Rev. B 83 (2011) 195102.

[70] A. Ruiz-Serrano, N. D. M. Hine, C.-K. Skylaris, Pulay forces from localized orbitals optimized in situ using a psinc basis set, J. Chem. Phys. 136 (2012) 234101.

[71] W. C. Swope, H. C. Andersen, P. H. Berens, K. R. Wilson, A computer simulation method for the calculation of equilibrium constants for the formation of physical clusters of molecules: Application to small water clusters, The Journal of Chemical Physics 76 (1) (1982) 637–649. arXiv:http://dx.doi.org/10.1063/1.442716, doi:10.1063/1.442716.
URL http://dx.doi.org/10.1063/1.442716

[72] S. Nosé, A unified formulation of the constant temperature molecular dynamics methods, The Journal of Chemical Physics 81 (1) (1984) 511–519. arXiv:http://dx.doi.org/10.1063/1.447334, doi:10.1063/1.447334.
URL http://dx.doi.org/10.1063/1.447334

[73] W. G. Hoover, Canonical dynamics: Equilibrium phase-space distributions, Phys. Rev. A 31 (1985) 1695–1697. doi:10.1103/PhysRevA.31.1695.
URL http://link.aps.org/doi/10.1103/PhysRevA.31.1695

[74] M. Parrinello, A. Rahman, Polymorphic transitions in single crystals: A new molecular dynamics method, Journal of Applied Physics 52 (12) (1981) 7182–7190. arXiv:http://dx.doi.org/10.1063/1.328693, doi:10.1063/1.328693.
URL http://dx.doi.org/10.1063/1.328693

[75] W. Shinoda, M. Shiga, M. Mikami, Rapid estimation of elastic constants by molecular dynamics simulation under constant stress, Phys. Rev. B 69 (2004)

134103. doi:10.1103/PhysRevB.69.134103.

URL http://link.aps.org/doi/10.1103/PhysRevB.69.134103